ACS Energy LETTERS

http://pubs.acs.org/journal/aelccp

Imaging Real-Time Amorphization of Hybrid Perovskite Solar Cells under Electrical Biasing

Min-cheol Kim,[†] Namyoung Ahn,[†] Diyi Cheng,[†] Mingjie Xu, So-Yeon Ham, Xiaoqing Pan, Suk Jun Kim, Yanqi Luo, David P. Fenning, Darren H. S. Tan, Minghao Zhang, Guomin Zhu, Kiwan Jeong, Mansoo Choi,* and Ying Shirley Meng*

Cite This: *ACS Energy Lett.* 2021, 6, 3530−3537

Read Online

ACCESS | Metrics & More | Article Recommendations | Supporting Information

ABSTRACT: **Perovskite solar cells have drawn much attention recently owing to their world-record-setting photovoltaic performances, whereas their practicality is still limited by the structural instability that often arises from ion migration and defect formation. Despite the general understanding that ion instability is a primary cause for degradation, there is no observation of structural transformation at the atomistic scale. Such observation is crucial to understand how instabilities are induced by external perturbations such as illumination or electrical bias, allowing researchers to devise effective strategies to mitigate them. Here, we designed an *in situ* transmission electron microscopy setup to enable real-time observation of amorphization in perovskite materials under electrical biasing. To reverse the device performance degradation due to such structural changes, the samples were heated at 50 °C and were found to recrystallize, effectively regaining their performance losses. This work presents vital insights on understanding ion-migration phenomena and addressing instability challenges of perovskite optoelectronics.**

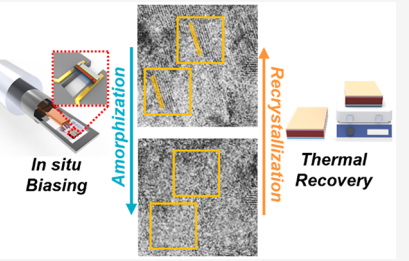

Since the onset of the 21st century, increasing demands for clean energy generation to displace traditional fossil fuels have generated an influx of interest in solar, wind, and other renewable sources of energy. Of these various technologies, photovoltaics are highly promising to achieve sustainable, safe, and robust energy to meet society's growing needs, by tapping only a fraction of the huge amounts of solar energy entering the Earth's atmosphere. Today, solar generation market products are still dominated by conventional silicon-based technologies. However, considering the demand for the development of energy devices that are flexible, lightweight, inexpensive, and highly efficient, there is still a high motivation for exploring the next generation of solar cells. As such, organic−inorganic hybrid perovskite solar cells (PSCs) have been extensively investigated in the past decade due to their high power conversion efficiencies (PCEs), exceeding 25.5% in recent reports,[1] as well as lower fabrication costs and emerging applications in tandem and flexible devices.[2−4] While initial reports indicated short device lifetime, that was mainly attributed to the material's sensitivity to heat, moisture, or other external factors which have been largely addressed with strategies such as introduction of more hydrophobic compounds or improved cell level designs with encapsulation.[5,6] However, the community soon realized that another significant cause of poor lifetime arises from the material's intrinsic degradation as well, believed to be a result of crystal phase instability and generation of defects. This instability is attributed to the fact that the ionic crystal exhibits excessive ion migration under light illumination and electrical bias.[7,8] Given that the application of any solar cells demands long-term operation under wide weather and climatic conditions, strategies to either mitigate or reverse these degradative effects are vital.

In PSCs, ion vacancies are easily generated since they have relatively low vacancy formation energies.[9,10] Under a potential bias, ions and vacancies migrate easily toward electrodes induced by Coulombic forces while the device is illuminated.[11−13] Namely, the charged ions (or carriers) will be simply governed by a drift-diffusion model. As a consequence, ion accumulation and charge carrier accumulation at the respective interfaces lead to performance degradation within just a few hours.[14,15] Fortunately, these devices with degraded performance can recover their initial capabilities if the ions or accumulated charges can be redistributed, which typically occurs after the device is stored in a dark state.[16,17] However, when this process is repeated over many cycles under periodic electrical bias, it has been found that the device eventually experiences

Received: August 14, 2021

https://doi.org/10.1021/acsenergylett.1c01707
ACS Energy Lett. 2021, 6, 3530−3537

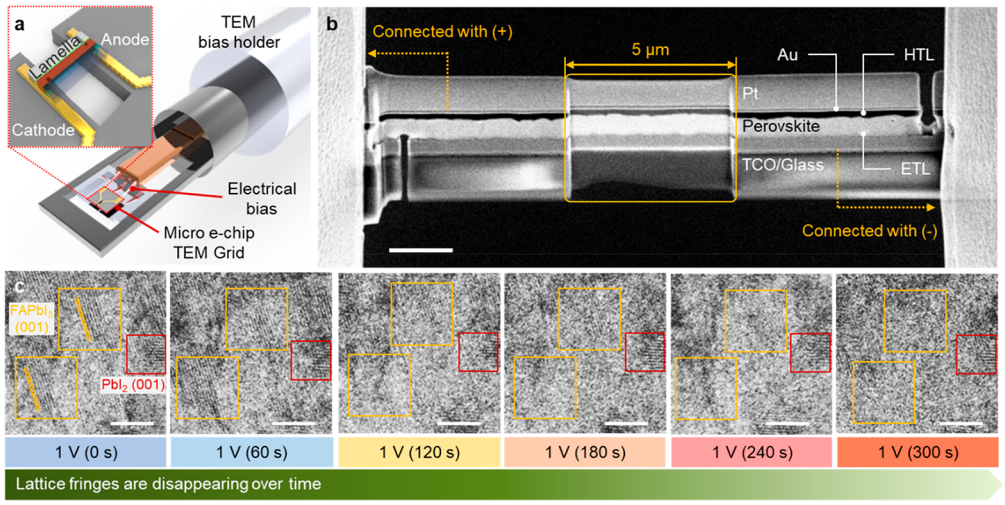

Figure 1. ***In situ*** **observation of changes in perovskite materials induced by electrical biases. (a) Schematic of** ***in situ*** **TEM sample configuration under electrical bias. A nano solar cell lamella is mounted on the micro e-chip TEM and stimulated with electrical bias in a TEM biasing holder. (b) SEM image of the nano solar cell lamella used for** ***in situ*** **observation prepared by FIB. The scale bar is 2 μm. (c) HRTEM image series of perovskite materials under 1 V electrical bias. The perovskite loses its crystallinity over time, as shown by the disappearance of lattice fringes in the yellow boxes. The lead iodide kept its structure intact, with lattice fringes present throughout the 5 min biasing.**

irreversible degradation, preventing its practical use in long-term devices.[15,18]

These degradation effects have been investigated to some extent in the literature and reported as a consequence of ion migration and segregation. Di Girolamo et al. recently reported the integrated intensity of main peaks using X-ray diffraction (XRD) patterns of PSCs and found decreases in intensities when the sample was biased at 1.2 V in the dark, concluding that perovskite amorphization occurred as a result of ion migration.[19] While these observations provide a clue on the amorphization effects under electrical bias, the structural transformation at the atomic level still remains unclear.[20−22] Alternatively, element-tracking techniques were previously employed to reveal that organic cations and halide anions migrate during device operation.[14,23,24] These experiments have collectively concluded that facile movements of halide anions impair the performance of PSCs, agreeing with past theoretical predictions using density functional theory calculations.[7,9,25] Although such interpretations can explain the reversible nature of ion redistribution, crystallographic transformation by ion migration is still not verified. Direct observation of ion migration at the atomistic scale is needed to provide evidence for ion-migration-induced amorphization. To this end, high-resolution transmission electron microscopy (HRTEM) imaging can potentially provide the missing knowledge and help gain fundamental understanding on such structural changes, phase transitions, and amorphization. Unfortunately, this is experimentally challenging to execute, due to the dynamic nature of perovskite materials' instability against the application of an external electrical bias, making it hard to capture without simultaneous electrical bias and imaging.

In this study, we addressed this limitation by designing an *in situ* TEM setup using a micro e-chip that can apply a stable electrical bias while imaging the bias-induced sample simultaneously. Accompanying selected area electron diffraction (SAED) analysis allows real-time observation of amorphization within the double-cation mixed perovskite materials under a 1 V forward bias. *Ex situ* XRD measurements support the bias-induced amorphization on the basis of reduced peak intensities after application of an electrical bias. Additionally, the effect of partial amorphization was examined via a light-induced degradation test; a forward bias induced by photovoltage led to faster performance decay compared to that of a controlled sample without electrical bias (short-circuited). To reverse these effects, mild heat treatment of the degraded sample at 50 °C was used to drive recrystallization of the amorphous phase, allowing it to regain its performance. Based on these observations, we propose a possible mechanism of the partial amorphization. This work demonstrates the ability to achieve real-time imaging of perovskite amorphization and provides an effective method to recover degraded performance of PSCs related to ion instability.

To study nanoscale changes of perovskite materials under electrical bias, we employed *in situ* TEM using a micro e-chip setup, where a stable electrical bias was applied to a nano solar cell TEM lamella (Figure 1a). As shown in Figure 1b and Figure S1, the nano solar lamella was prepared using a focused ion beam (FIB) methodology developed by Lee et al.[26] The lamella was then mounted between the electrodes of an e-chip. In order to apply an electrical bias through the perovskite layer without shorting the cell, columns were cut at the top-right corner and bottom-left corner of the lamella.[51] The middle region (5 μm in length) was thinned down to around 120 nm in thickness to facilitate TEM observation. Details of the fabrication procedure of the nano solar cell and electrical connection verification can be found in Figures S2 and S3. We can notice a rectification effect of the TEM sample which verifies the application of electrical bias from the external power source. Note that the voltage bias applied in this experiment was set to mimic the photovoltage of an open-circuited PSC device under one sun illumination. The sample was prepared at the pristine state and was not pre-biased before the measurement.

First, the effect of a forward bias (1 V for 5 min) on the cross-sectional morphology was examined, whereupon no morphological change or damage was observed, indicating the stability of the nano solar cell under such beam conditions. (For details, see Video S1 and Figure S4.) At the higher magnification, obvious bias-induced changes were presented in several domains of perovskite nanocrystals, as can be seen in Video S2 and Figure

https://doi.org/10.1021/acsenergylett.1c01707
ACS Energy Lett. 2021, 6, 3530−3537

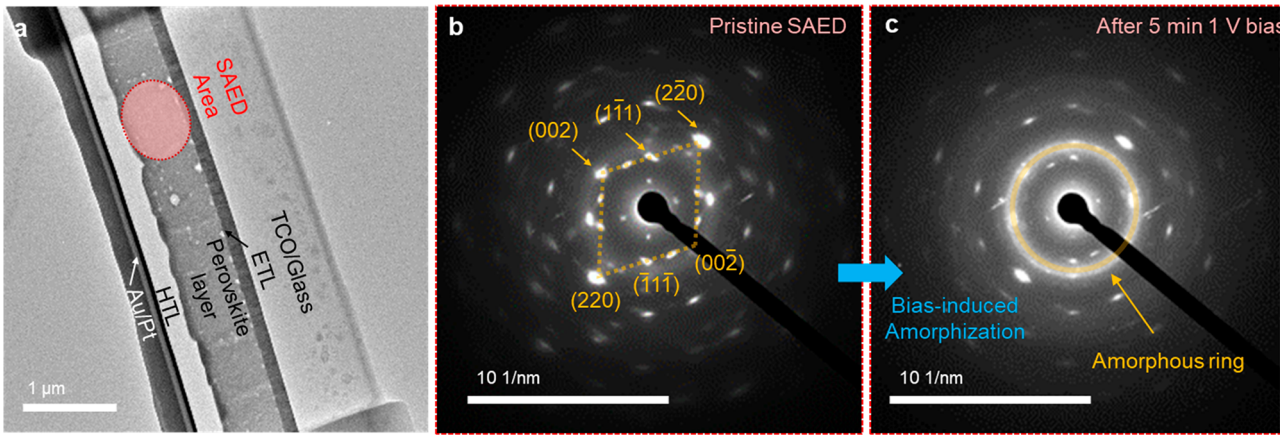

Figure 2. Verification of perovskite amorphization induced by electrical bias. (a) TEM image of nano solar cell indicating the locations of the SAED area. SAED patterns of perovskite materials at the highlighted region (b) before and (c) after 5 min of forward bias (1 V) without beam radiation.

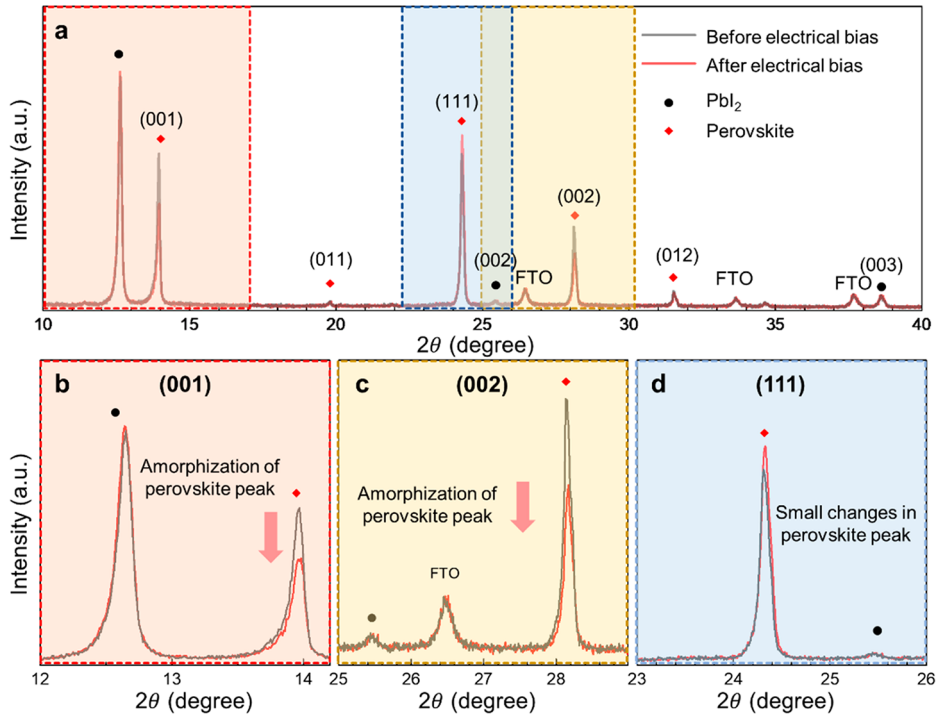

Figure 3. Perovskite film amorphization under electrical bias verified by XRD. (a) XRD patterns of perovskite materials at pristine state (black line) and after application of forward bias (1 V) for 10 min (red line). The measured PSCs are rinsed with chlorobenzene to remove Spiro-MeOTAD and the Au layer. Zoomed-in XRD patterns highlighting the differences near the (b) (001), (c) (002), and (d) (111) peaks of perovskite materials, where PbI_2 and perovskite species are indicated by black dots and red diamonds, respectively.

S5. To obtain nanoscale structural information, HRTEM images were acquired, as shown in Figure 1c and Video S3. Lattice fringes of perovskite crystals at 0 s were seen to gradually disappear (highlighted region in yellow boxes of Figure 1c) and became completely absent after 300 s of continuous 1 V forward bias. Real-time fading of specific lattice fringes by electrical bias implied amorphization of perovskite nanocrystals; such structural changes were not reported before in organic−inorganic hybrid perovskite materials at the atomic scale. A further comparison between the HRTEM images at 0 and 300 s is shown in Figure S6, where reduced fast Fourier transform (FFT) patterns were sampled at different regions. Interestingly, the lattice fringes in the yellow boxes disappeared after 5 min of electrical bias; however, those in the red box retained the majority of their crystalline characteristics post-bias. A detailed analysis showed that the *d*-spacings of the lattice fringes in the yellow boxes and red boxes corresponded to the (001) plane of the perovskite crystal ($(FAPbI_3)_x(MAPbBr_3)_{1-x}$) (6.36 Å)[27] and the (001) plane of PbI_2 (6.96 Å),[28] indicating that the amorphization occurred only in the perovskite phase.

According to previous TEM studies on perovskite materials, ion beam exposure during sample preparation and electron beam irradiation during observation may lead to detrimental damage to the materials.[29,50] Considering an electron dose rate of ~85 e^{-1} $Å^{-2}$ s^{-1} for each image, our perovskite materials may have experienced a certain amount of beam damage during the *in situ* TEM observation. Based on the *in situ* TEM images in Figure 1 and videos in the Supporting Information, therefore, it

https://doi.org/10.1021/acsenergylett.1c01707
ACS Energy Lett. 2021, 6, 3530−3537

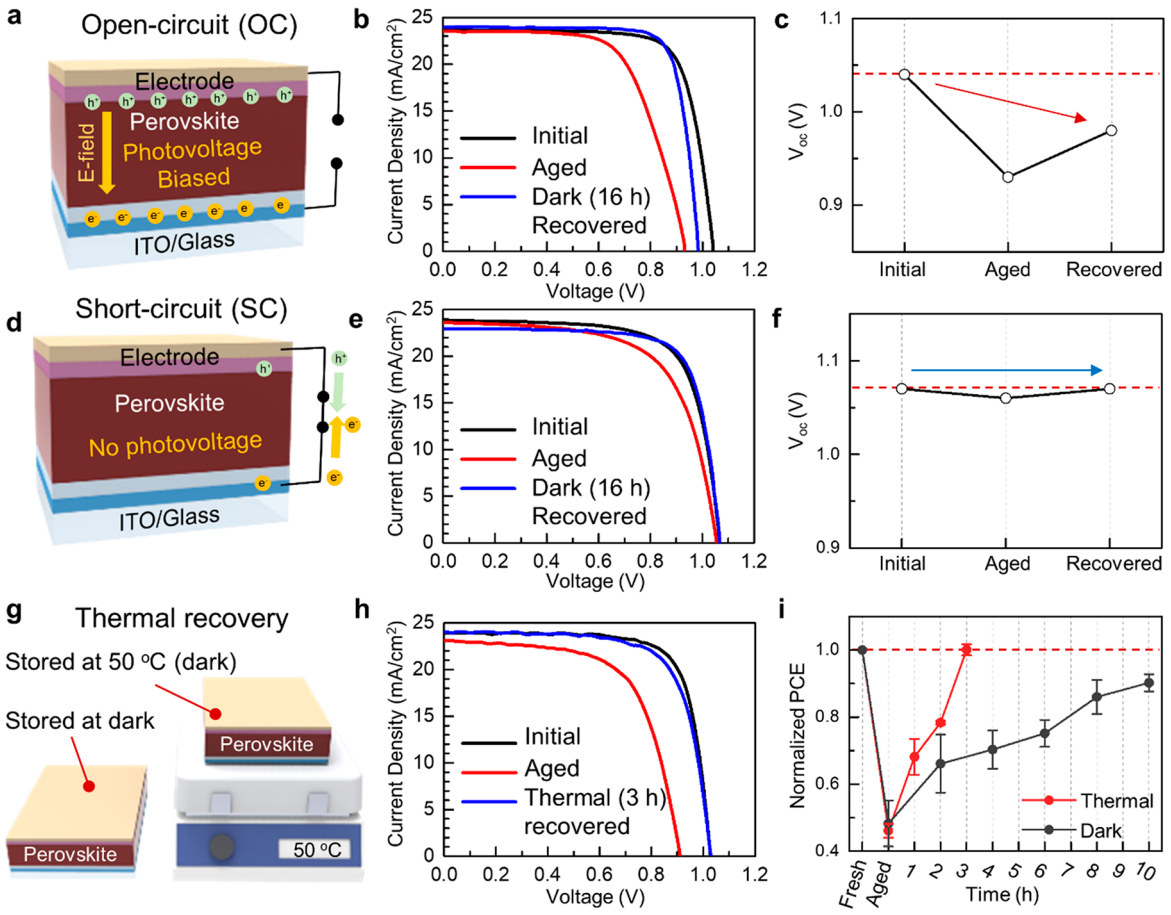

Figure 4. Device performance degradation under electrical bias and dark/thermal recovery. (a, d) Schematics of PSCs under light illumination at open-circuit (OC) and short-circuit (SC) conditions. The photovoltage generated at OC conditions can induce charge accumulation that leads to the formation of an internal electric field at the perovskite layer. (b, e) Current density (J)−voltage (V) curves of PSCs at the initial state (black line), after 16 h of aging (red line), and after 16 h of recovery in the dark (blue line) at OC and SC conditions, respectively. (c, f) Evolution of open-circuit voltage (V_{oc}) from the initial state to the recovered state for PSCs at OC and SC conditions. Black solid lines are guides to the eye. (g) Schematic of dark recovery and thermal recovery of degraded PSCs. (h) J−V curves of PSCs at initial state (black line), after 16 h of aging at OC condition (red line), and after 3 h of recovery at 50 °C. (i) Comparison of thermal and dark recovery of degraded PSCs.

is fair to claim that the perovskite materials underwent amorphization as a consequence of both electrical bias application and electron beam radiation. It is also noted that such observations might be a result of the sample tilting during the continuous observation. In order to check the beam damage effect, we radiated the electron beam on the perovskite TEM lamella at the same beam conditions (Figure S7 and Video S4). No changes in the lattice fringes were observed under continuous electron beam irradiation for 5 min, during which the FFT patterns and peak intensities remain the same (Figure S8), while they respectively disappeared and diminished under the electrical bias, as shown in Figure S9. As a result, we noticed a clear difference between the two *in situ* TEM observation conditions, with and without electrical bias. However, since the electron beam damage might shift the degradation mechanism of perovskite materials, the effect of electrical bias on perovskite materials needs to be isolated for further investigation.

In that sense, SAED patterns were acquired to provide essential information to correlate the lattice fringe disappearance with the partial amorphization of the perovskite materials. Figure 2 shows the SAED patterns to verify the effect of electrical bias on perovskite materials. Detailed information on the indexing of the SAED patterns is presented in Figure S10. We can notice that PbI_2 and perovskite crystals are overlapped, which results from the sequential deposition fabrication process and ion-beam- or electron-beam-induced damage during the sample preparation. But here, we can elicit the electrical bias effect since application of electrical bias was the only stimulus to the perovskite materials during the experiments. Significant changes in SAED patterns were noticed when 1 V of electrical bias was applied for 5 min in the absence of electron beam irradiation (Figure 2b,c). The amorphous ring became obviously more pronounced in the SAED pattern, which confirms the amorphization effect of electrical bias without electron beam irradiation. Collected SAED patterns are indexed from crystal structure data of perovskite and compared to simulated electron diffraction patterns (Figure S11).[27] The amorphous ring mostly overlapped, with d-spacing of (002), diffraction spots of perovskite in the SAED patterns, which is strong evidence of the partial amorphization.

Since observations made in the *in situ* TEM can be attributed to localized phenomena, bulk-scale characterization was also conducted to confirm the partial amorphization at the device level. *Ex situ* XRD measurements of the fresh and post-bias device (1 V for 10 min) were conducted and are shown in Figure 3. Magnified XRD patterns in Figure 3b,c show that the forward bias led to a significant decrease in peak intensities of the (001) and (002) planes while peak intensities of PbI_2 and FTO

https://doi.org/10.1021/acsenergylett.1c01707
ACS Energy Lett. 2021, 6, 3530−3537

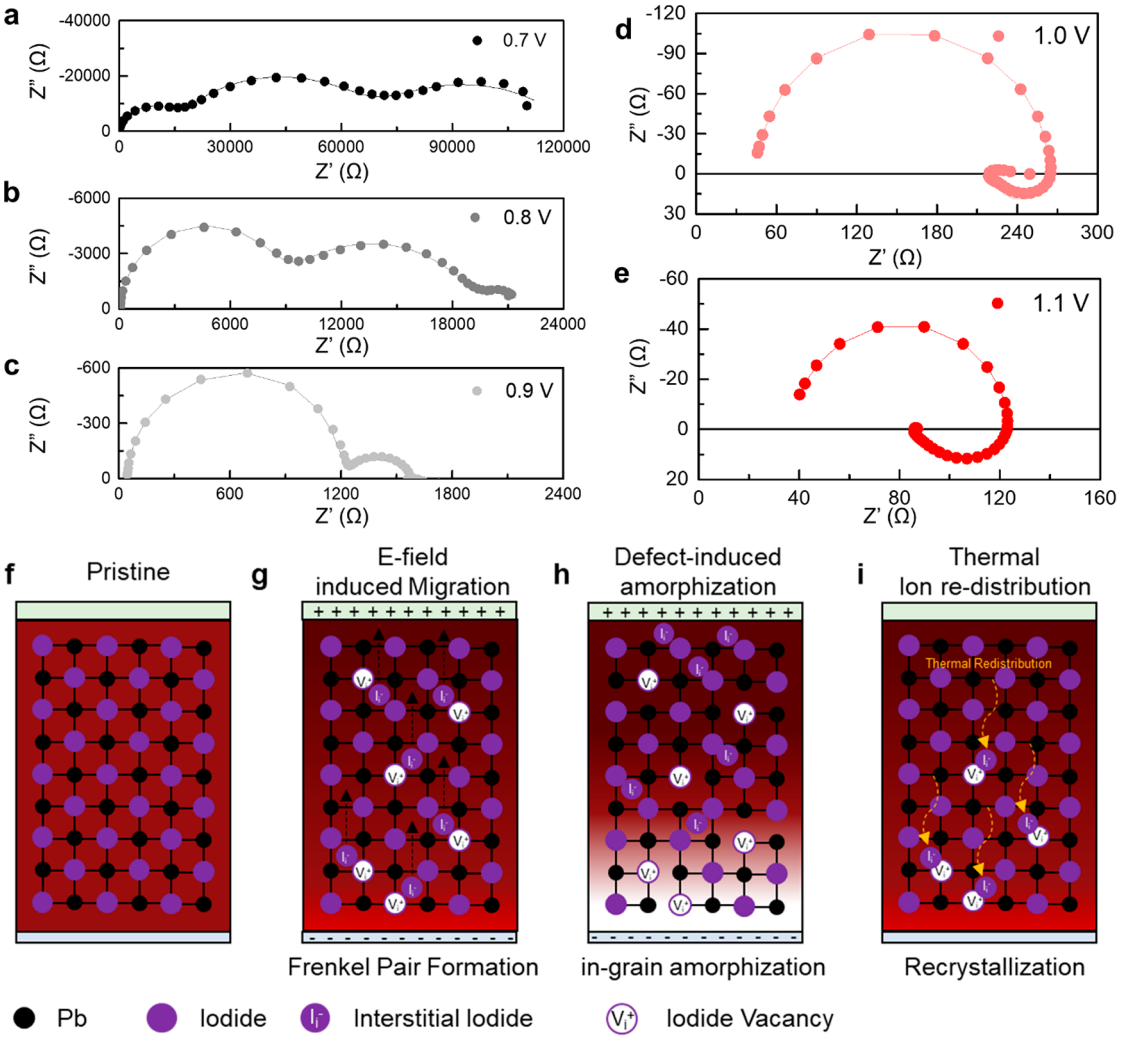

Figure 5. Evidence for ion migration and mechanism of amorphization from the ion migration. EIS plots of the PSCs measured from 1 MHz to 100 mHz with forward bias of (a) 0.7, (b) 0.8, (c) 0.9, (d) 1.0, and (e) 1.1 V in dark conditions. Inductance (or negative capacitance) occurred only when the forward bias exceeds 1.0 V, verifying the ion migration. (f–i) Proposed mechanism for ion-migration-induced partial amorphization of perovskite materials and the recovery from thermal ion redistribution.

remained the same, confirming amorphization of the perovskite phase during the electrical biasing. During bias-induced amorphization, a phase transition to the δ-phase did not occur, as shown in Figure S12, which means the structural change under electrical bias is not from either decomposition or a phase transition but from the amorphization.[30] Peak broadening is accompanied by a decrease of peak intensity during the process, which is clear evidence for the amorphization (Table S1). Integral breadths for amorphized lattice planes increased significantly after the application of electrical bias, while those for PbI_2 were almost not changed. These *in situ* TEM and *ex situ* XRD results imply that partial amorphization of the perovskite film is induced by electrical forward bias, consistent with previous studies.[19,21] Additionally, this affirms the correlation between atomic structural changes and the performance degradation of photovoltaic devices under the electrical bias.

In order to address PSCs' long-term stability issues, it is essential to understand how such partial amorphization takes place under light illumination as well as affects photovoltaic performance during an actual operation. To evaluate this, a degradation test setup was used to apply different electrical conditions, i.e., open-circuit (OC) and short-circuit (SC), as illustrated in Figure 4a,d to explore the effects of amorphization on the PSCs' performance. When both PSCs were placed under continuous one sun illumination, a photovoltage (~1 V) was developed in the OC device and charge carriers accumulated at the interfaces between the perovskite and transport layers, creating a photovoltage-induced electric field for charged ions pointing from anode to cathode.[31,32] On the other hand, charge carriers did not accumulate at the interfaces in the SC device; therefore, no induced electrical potential between cathode and anode was applied to the charged ions. In other words, a photovoltage-induced electric field due to charge accumulation was only generated in OC conditions, which was equivalent to the forward bias to the device, analogous to that during the *in situ* TEM and *ex situ* XRD measurements. Considering that the injection of carriers from either external electrical bias or light illumination allowed the ions to migrate more freely, applying an electrical bias or using the induced electric field from the charge accumulation could give the same structural changes caused by ion migration.[33] A degradation test was conducted in a pure nitrogen environment to exclude the effect of surrounding reactive molecules (such as oxygen) and moisture. Figure 4b,e

https://doi.org/10.1021/acsenergylett.1c01707
ACS Energy Lett. 2021, 6, 3530−3537

shows changes in the $J-V$ curves of the OC and SC devices, respectively. Photovoltaic parameters calculated from each $J-V$ curve are listed in Table S2. For both conditions, performance was degraded when the device was illuminated and was restored after recovery in the dark due to photo-activated reversible ion migration.[17] However, the forward bias in the OC case caused dramatic changes during degradation as compared to the SC case, consistent with previous studies.[16,17,34,35] Specifically, the open-circuit voltage (V_{oc}) largely decreased after 16 h of light soaking and did not return to the original value after recovery in darkness, which indicates that the defect concentration and the crystallinity of the perovskite film were mainly influenced by forward bias (see Figure 4c).[36,37] On the other hand, the V_{oc} values hardly changed in the SC case and recovered to the initial V_{oc} after 16 h, as shown in Figure 4f. Unlike the V_{oc} values, the degraded PCE of perovskite devices in both OC and SC cases recovered to the initial PCE, as shown in Figure S13. The partially amorphous phase may be recrystallized spontaneously while the device is stored in the dark under an inert atmosphere and ambient temperature, which can possibly lead to performance recovery. As with the electrical bias application effect from the photovoltage, a performance degradation test under foward bias from the external power sources in the dark state also exhibits the same degradation and recovery trend (Figure S14). This validates that the photo-induced internal electric field has an equivalent impact on the partial amorphization from the ion migration with the external electrical bias. To validate the parity of the *in situ* TEM observation and device stability test, we assumed that the majority of degradation was attributed to ion migration under electrical bias at both conditions. Although the two cases have different geometric and electrical conditions, this seems highly plausible, given that they showed consistent crystallinity transitions.

Considering that degradation as a result of ion migration can be reversed with ion redistribution under darkness,[14,19] supplying additional thermal energy should promote such ion redistribution and hasten the recovery process. Thus, a thermal recovery test was conducted on the degraded devices by heating at 50 °C in the dark (Figure 4g). The degraded PSCs under continuous light illumination were restored to the initial performance within just 3 h when they were heated at 50 °C in darkness (Figure 4h,i). Note that performance was not fully recovered even after 10 h of storage in the dark at room temperature, demonstrating the effectiveness of applying mild heating. These results indicate that thermal energy facilitated the prompt recovery process of degraded PSCs through recrystallization of amorphous perovskite. Investigation on the crystallinity by XRD measurement verified the recrystallization by the recovery process (Figure S15), indicating that the bias-induced degradation of perovskite materials can be recovered through recrystallization. There is a possibility of reversible recovery of performance and perovskite crystallinity through reformation by the reaction of PbI_2 and organic halides. However, such reformation would be difficult since organic cations and halide anions migrated to both sides under electrical bias; therefore, the amorphization and recrystallization process prevails in this case. Although a reversible change in the PCEs of PSCs has been reported in previous studies,[14,16,17,38−40] this work offers new a direct observation of dynamic changes in the crystallinity of perovskite materials as a result of forward bias. Moreover, mild heating was found to be an effective solution to expedite performance recovery under darkness, potentially extending the practical lifetime of PSC devices if they can be recovered at increased temperatures periodically during the nighttime.

Next, to elucidate the electrochemical effects of ion migration (or possible partial amorphization), electrical-bias-induced ion migration inside the perovskite device was investigated via electrochemical impedance spectroscopy (EIS) and energy-dispersive X-ray spectroscopy (EDS) measurements. After various magnitudes of forward bias were applied, an inductance response (or negative capacitance) was observed at low frequencies for bias greater than 1 V, as shown in Figure 5. Since the device was measured and stored in the dark, there would be no influence from photogenerated charges and generation of electrical potential. While the device was biased, the electrical circuit of the device was merely composed of resistances and capacitances, similar to that in general perovskite devices (Figure 5a−c).[41] Thus, the new inductance component (negative capacitance) after forward bias beyond 1 V would be indicative of a significant material transformation in terms of ionic migration (Figure 5d,e).[42−45] Notably, such a remarkable transformation was possibly associated with the partial amorphization based on our *in situ* TEM observations (see Figure 2).

Emergence of the negative capacitance at forward bias over 1 V clearly implies that ions are migrated to interfaces via the electric field, thereby forming a reverse surface charging as a source of negative capacitance.[46] This was likely related with the inverted hysteresis behavior of the aged device, where the forward-scan PCE (scan from J_{sc} to V_{oc}) became larger than the reverse-scan one (scan from V_{oc} to J_{sc}) (see Figure S16). A perovskite device that initially exhibited normal hysteresis (the reverse-scan PCE is larger than the forward-scan one) showed inverted hysteresis after 16 h of aging under light illumination and OC condition. Since the hysteresis behavior of PSCs was attributed to the ion migration,[8,47] the change of the hysteresis behavior was related with the mobile ions, verified by the negative capacitance that developed under the forward bias over 1 V.

From the above characterization and analysis results, a possible mechanism for the partial amorphization coupled with dynamics of ion migration is proposed. Although some defects with low defect formation energies are intrinsically formed in pristine perovskite crystals, this still represents a low fraction of defect density (Figure 5f). After an external electric field is applied via forward bias or illumination, the formation of Frenkel pairs (V_I^+/I_i^-) will be more energetically favorable due to their low defect formation energy (Figure 5g).[7] The newly formed interstitial defects and vacancies are the most active species during electric-field-induced ion migration.[13] Our EDS results showed that iodine distribution exhibited the most drastic change, whereas other components of perovskite crystals remained relatively unchanged after the forward bias (Figure S17). Moreover, iodine accumulation near the cathode interface was observed, as shown in Figure S18, suggesting that negatively charged interstitial iodine defects migrated under the driving force of the electric field. Not only the single-line EDS scan along the perovskite layer but also the averaged plots extracted from the 2D EDS mapping validate the ion migration along the perovskite layer and localized iodide ion at the cathode region (Figure S19). As a result of continuous ion migration, density distributions of iodide interstitials or vacancies will no longer be uniform across the perovskite layer, which would possibly lead to defect-induced partial amorphization.[48,49] The corresponding planes, which always contain iodides, will experience loss of

https://doi.org/10.1021/acsenergylett.1c01707
ACS Energy Lett. 2021, 6, 3530−3537

periodicity due to the increased iodide defects under electrical bias. In contrast, the (111) groups consist of (111) Pb and (111) FAI_3 planes separately, which means the periodicity can remain as long as the (111) Pb plane is still alive. Consequently, amorphization would be more favorable with the increased defect concentrations in the (001) and (002) groups. Finally, these degradation effects can be reversed by resting the device under dark conditions, which allows ion redistribution to occur (Figure 5i). To increase the rate of recovery, the process can be facilitated by adding mild thermal energy, as shown in the results (Figure 4i).

In conclusion, *in situ* HRTEM was used to achieve direct real-time observation of perovskite crystal amorphization. A lamella of a nano solar cell was prepared using FIB and mounted on an e-chip to allow us to observe structural changes under a constant forward bias of 1 V. Under bias, the disappearance of lattice fringes in the HRTEM images, accompanied with the manifestation of a clear amorphous ring in the SAED patterns, was observed, which is evidence of perovskite amorphization. These bias-induced perovskite amorphization results were complemented with bulk XRD measurements that showed a decrease of the peak intensities of the major perovskite planes, while other peaks associated with PbI_2 remained unchanged. A possible mechanism of amorphization based on halide ion migration and defect generation is proposed. As ion migration was identified as the primary cause of performance degradation, the performance recovery rate was found to improve upon heating the PSC device at 50 °C to promote ion redistribution, where the device was fully recovered after only 3 h. Overall, this study provides unprecedented observations of atomic-scale transitions during bias-induced degradation. These observations reveal that, although perovskite amorphization results in degradation in PSC devices, it can be effectively recovered through a recrystallization process under mild conditions, reflecting a realistic strategy to maintain long-term device performance.

■ ASSOCIATED CONTENT

Supporting Information

The Supporting Information is available free of charge at https://pubs.acs.org/doi/10.1021/acsenergylett.1c01707.

Detailed description of the experimental methods, additional data, including Figures S1−S19 and Tables S1 and S2, and details of author contributions (PDF)

Video S1. Low-magnification in situ biasing at 1 V for 5 min (MP4)

Video S2. Medium-magnification in situ biasing at 1 V for 5 min (MP4)

Video S3. High-magnification in situ biasing at 1 V for 5 min (MP4)

Video S4. 5-minute continuous electron beam irradiation (MP4)

■ AUTHOR INFORMATION

Corresponding Authors

Mansoo Choi − *Global Frontier Center for Multiscale Energy Systems and Department of Mechanical Engineering, Seoul National University, Seoul 08826, Republic of Korea;* orcid.org/0000-0003-3198-6899; Email: mchoi@snu.ac.kr

Ying Shirley Meng − *Department of NanoEngineering and Materials Science and Engineering Program, University of California San Diego, La Jolla, California 92093, United States;* orcid.org/0000-0001-8936-8845; Email: shmeng@ucsd.edu

Authors

Min-cheol Kim − *Department of NanoEngineering, University of California San Diego, La Jolla, California 92093, United States; School of Mechanical Engineering, Pusan National University, Busan 46241, Korea*

Namyoung Ahn − *Global Frontier Center for Multiscale Energy Systems, Seoul National University, Seoul 08826, Republic of Korea*

Diyi Cheng − *Materials Science and Engineering Program, University of California San Diego, La Jolla, California 92093, United States*

Mingjie Xu − *Irvine Materials Research Institute, University of California Irvine, Irvine, California 92697, United States*

So-Yeon Ham − *Materials Science and Engineering Program, University of California San Diego, La Jolla, California 92093, United States*

Xiaoqing Pan − *Irvine Materials Research Institute, University of California Irvine, Irvine, California 92697, United States*

Suk Jun Kim − *School of Energy, Materials and Chemical Engineering, Korea University of Technology and Education, Cheonan 31253, Republic of Korea*

Yanqi Luo − *Department of NanoEngineering, University of California San Diego, La Jolla, California 92093, United States;* orcid.org/0000-0001-5624-9583

David P. Fenning − *Department of NanoEngineering, University of California San Diego, La Jolla, California 92093, United States;* orcid.org/0000-0002-4609-9312

Darren H. S. Tan − *Department of NanoEngineering, University of California San Diego, La Jolla, California 92093, United States*

Minghao Zhang − *Department of NanoEngineering, University of California San Diego, La Jolla, California 92093, United States*

Guomin Zhu − *Department of NanoEngineering, University of California San Diego, La Jolla, California 92093, United States*

Kiwan Jeong − *Global Frontier Center for Multiscale Energy Systems, Seoul National University, Seoul 08826, Republic of Korea*

Complete contact information is available at: https://pubs.acs.org/10.1021/acsenergylett.1c01707

Author Contributions

†M.K., N.A., and D.C. contributed equally to this paper.

Notes

The authors declare no competing financial interest.

■ ACKNOWLEDGMENTS

This work was supported by a California Energy Commission EPIC Advance Breakthrough Award (EPC-16-050). This work was also supported by National Research Foundation of Korea (NRF) Global Frontier R&D Program of the Center for Multiscale Energy Systems (2012M3A6A7054855). The authors would like to acknowledge the financial support received for this study from the U.S. Department of Energy, Office of Basic Energy Sciences, under Award Number DE-SC0002357 (program manager Dr. Jane Zhu). The work done at the

University of California Irvine was supported by the Irvine Materials Research Institute (IMRI).

REFERENCES

(1) National Renewable Energy Laboratory. Best Research-Cell Efficiency Chart, https://www.nrel.gov/pv/cell-efficiency.html (accessed: March 2021).
(2) Kim, D.; Jung, H. J.; Park, I. J.; Larson, B. W.; Dunfield, S. P.; Xiao, C.; Kim, J.; Tong, J.; Boonmongkolras, P.; Ji, S. G.; Zhang, F.; Pae, S. R.; Kim, M.; Kang, S. B.; Dravid, V.; Berry, J. J.; Kim, J. Y.; Zhu, K.; Kim, D. H.; Shin, B. *Science* **2020**, *368*, 155.
(3) Lee, G.; Kim, M.-c.; Choi, Y. W.; Ahn, N.; Jang, J.; Yoon, J.; Kim, S. M.; Lee, J.-G.; Kang, D.; Jung, H. S.; Choi, M. *Energy Environ. Sci.* **2019**, *12*, 3182.
(4) Song, Z.; McElvany, C. L.; Phillips, A. B.; Celik, I.; Krantz, P. W.; Watthage, S. C.; Liyanage, G. K.; Apul, D.; Heben, M. J. *Energy Environ. Sci.* **2017**, *10*, 1297.
(5) Zuo, L.; Guo, H.; deQuilettes, D. W.; Jariwala, S.; De Marco, N.; Dong, S.; DeBlock, R.; Ginger, D. S.; Dunn, B.; Wang, M.; Yang, Y. *Science Advances* **2017**, *3*, e1700106.
(6) Han, Y.; Meyer, S.; Dkhissi, Y.; Weber, K.; Pringle, J. M.; Bach, U.; Spiccia, L.; Cheng, Y.-B. *J. Mater. Chem. A* **2015**, *3*, 8139.
(7) Eames, C.; Frost, J. M.; Barnes, P. R. F.; O'Regan, B. C.; Walsh, A.; Islam, M. S. *Nat. Commun.* **2015**, *6*, 7497.
(8) Calado, P.; Telford, A. M.; Bryant, D.; Li, X.; Nelson, J.; O'Regan, B. C.; Barnes, P. R. F. *Nat. Commun.* **2016**, *7*, 13831.
(9) Azpiroz, J. M.; Mosconi, E.; Bisquert, J.; De Angelis, F. *Energy Environ. Sci.* **2015**, *8*, 2118.
(10) Shao, Y.; Xiao, Z.; Bi, C.; Yuan, Y.; Huang, J. *Nat. Commun.* **2014**, *5*, 5784.
(11) Xiao, Z.; Yuan, Y.; Shao, Y.; Wang, Q.; Dong, Q.; Bi, C.; Sharma, P.; Gruverman, A.; Huang, J. *Nat. Mater.* **2015**, *14*, 193.
(12) Leijtens, T.; Hoke, E. T.; Grancini, G.; Slotcavage, D. J.; Eperon, G. E.; Ball, J. M.; De Bastiani, M.; Bowring, A. R.; Martino, N.; Wojciechowski, K.; McGehee, M. D.; Snaith, H. J.; Petrozza, A. *Adv. Energy Mater.* **2015**, *5*, 1500962.
(13) Yuan, Y.; Huang, J. *Acc. Chem. Res.* **2016**, *49*, 286.
(14) Domanski, K.; Roose, B.; Matsui, T.; Saliba, M.; Turren-Cruz, S.-H.; Correa-Baena, J.-P.; Carmona, C. R.; Richardson, G.; Foster, J. M.; De Angelis, F.; Ball, J. M.; Petrozza, A.; Mine, N.; Nazeeruddin, M. K.; Tress, W.; Grätzel, M.; Steiner, U.; Hagfeldt, A.; Abate, A. *Energy Environ. Sci.* **2017**, *10*, 604.
(15) Ahn, N.; Kwak, K.; Jang, M. S.; Yoon, H.; Lee, B. Y.; Lee, J.-K.; Pikhitsa, P. V.; Byun, J.; Choi, M. *Nat. Commun.* **2016**, *7*, 13422.
(16) Domanski, K.; Alharbi, E. A.; Hagfeldt, A.; Grätzel, M.; Tress, W. *Nature Energy* **2018**, *3*, 61.
(17) Nie, W.; Blancon, J.-C.; Neukirch, A. J.; Appavoo, K.; Tsai, H.; Chhowalla, M.; Alam, M. A.; Sfeir, M. Y.; Katan, C.; Even, J.; Tretiak, S.; Crochet, J. J.; Gupta, G.; Mohite, A. D. *Nat. Commun.* **2016**, *7*, 11574.
(18) Kim, M.-c.; Ahn, N.; Lim, E.; Jin, Y. U.; Pikhitsa, P. V.; Heo, J.; Kim, S. K.; Jung, H. S.; Choi, M. *J. Mater. Chem. A* **2019**, *7*, 12075.
(19) Di Girolamo, D.; Phung, N.; Kosasih, F. U.; Di Giacomo, F.; Matteocci, F.; Smith, J. A.; Flatken, M. A.; Köbler, H.; Turren Cruz, S. H.; Mattoni, A.; Cinà, L.; Rech, B.; Latini, A.; Divitini, G.; Ducati, C.; Di Carlo, A.; Dini, D.; Abate, A. *Adv. Energy Mater.* **2020**, *10*, 2000310.
(20) Jeangros, Q.; Duchamp, M.; Werner, J.; Kruth, M.; Dunin-Borkowski, R. E.; Niesen, B.; Ballif, C.; Hessler-Wyser, A. *Nano Lett.* **2016**, *16*, 7013.
(21) Kim, D.; Yun, J. S.; Sharma, P.; Lee, D. S.; Kim, J.; Soufiani, A. M.; Huang, S.; Green, M. A.; Ho-Baillie, A. W. Y.; Seidel, J. *Nat. Commun.* **2019**, *10*, 444.
(22) Bischak, C. G.; Hetherington, C. L.; Wu, H.; Aloni, S.; Ogletree, D. F.; Limmer, D. T.; Ginsberg, N. S. *Nano Lett.* **2017**, *17*, 1028.
(23) Luo, Y.; Khoram, P.; Brittman, S.; Zhu, Z.; Lai, B.; Ong, S. P.; Garnett, E. C.; Fenning, D. P. *Adv. Mater.* **2017**, *29*, 1703451.
(24) Wang, R.; Xue, J.; Meng, L.; Lee, J.-W.; Zhao, Z.; Sun, P.; Cai, L.; Huang, T.; Wang, Z.; Wang, Z.-K.; Duan, Y.; Yang, J. L.; Tan, S.; Yuan, Y.; Huang, Y.; Yang, Y. *Joule* **2019**, *3*, 1464.
(25) Haruyama, J.; Sodeyama, K.; Han, L.; Tateyama, Y. *J. Am. Chem. Soc.* **2015**, *137*, 10048.
(26) Lee, J. Z.; Wynn, T. A.; Meng, Y. S.; Santhanagopalan, D. *J. Visualized Exp.* **2018**, e56259.
(27) Huang, Y.; Li, L.; Liu, Z.; Jiao, H.; He, Y.; Wang, X.; Zhu, R.; Wang, D.; Sun, J.; Chen, Q.; Zhou, H. *J. Mater. Chem. A* **2017**, *5*, 8537.
(28) Popov, G.; Mattinen, M.; Hatanpää, T.; Vehkamäki, M.; Kemell, M.; Mizohata, K.; Räisänen, J.; Ritala, M.; Leskelä, M. *Chem. Mater.* **2019**, *31*, 1101.
(29) Chen, S.; Gao, P. *J. Appl. Phys.* **2020**, *128*, 010901.
(30) Li, Z.; Yang, M.; Park, J.-S.; Wei, S.-H.; Berry, J. J.; Zhu, K. *Chem. Mater.* **2016**, *28*, 284.
(31) Chen, B.; Rudd, P. N.; Yang, S.; Yuan, Y.; Huang, J. *Chem. Soc. Rev.* **2019**, *48*, 3842.
(32) Bae, S.; Kim, S.; Lee, S.-W.; Cho, K. J.; Park, S.; Lee, S.; Kang, Y.; Lee, H.-S.; Kim, D. *J. Phys. Chem. Lett.* **2016**, *7*, 3091.
(33) Kerner, R. A.; Rand, B. P. *J. Phys. Chem. Lett.* **2018**, *9*, 132.
(34) Duong, T.; Mulmudi, H. K.; Wu, Y.; Fu, X.; Shen, H.; Peng, J.; Wu, N.; Nguyen, H. T.; Macdonald, D.; Lockrey, M.; White, T. P.; Weber, K.; Catchpole, K. *ACS Appl. Mater. Interfaces* **2017**, *9*, 26859.
(35) Bryant, D.; Aristidou, N.; Pont, S.; Sanchez-Molina, I.; Chotchunangatchaval, T.; Wheeler, S.; Durrant, J. R.; Haque, S. A. *Energy Environ. Sci.* **2016**, *9*, 1655.
(36) Tress, W.; Yavari, M.; Domanski, K.; Yadav, P.; Niesen, B.; Correa Baena, J. P.; Hagfeldt, A.; Graetzel, M. *Energy Environ. Sci.* **2018**, *11*, 151.
(37) Stranks, S. D. *ACS Energy Letters* **2017**, *2*, 1515.
(38) Saliba, M.; Matsui, T.; Domanski, K.; Seo, J.-Y.; Ummadisingu, A.; Zakeeruddin, S. M.; Correa-Baena, J.-P.; Tress, W. R.; Abate, A.; Hagfeldt, A.; Grätzel, M. *Science* **2016**, *354*, 206.
(39) Bag, M.; Renna, L. A.; Adhikari, R. Y.; Karak, S.; Liu, F.; Lahti, P. M.; Russell, T. P.; Tuominen, M. T.; Venkataraman, D. *J. Am. Chem. Soc.* **2015**, *137*, 13130.
(40) Anaraki, E. H.; Kermanpur, A.; Steier, L.; Domanski, K.; Matsui, T.; Tress, W.; Saliba, M.; Abate, A.; Grätzel, M.; Hagfeldt, A.; Correa-Baena, J.-P. *Energy Environ. Sci.* **2016**, *9*, 3128.
(41) Zarazua, I.; Han, G.; Boix, P. P.; Mhaisalkar, S.; Fabregat-Santiago, F.; Mora-Seró, I.; Bisquert, J.; Garcia-Belmonte, G. *J. Phys. Chem. Lett.* **2016**, *7*, 5105.
(42) Guerrero, A.; Garcia-Belmonte, G.; Mora-Sero, I.; Bisquert, J.; Kang, Y. S.; Jacobsson, T. J.; Correa-Baena, J.-P.; Hagfeldt, A. *J. Phys. Chem. C* **2016**, *120*, 8023.
(43) Moia, D.; Gelmetti, I.; Calado, P.; Fisher, W.; Stringer, M.; Game, O.; Hu, Y.; Docampo, P.; Lidzey, D.; Palomares, E.; Nelson, J.; Barnes, P. R. F. *Energy Environ. Sci.* **2019**, *12*, 1296.
(44) Ghahremanirad, E.; Bou, A.; Olyaee, S.; Bisquert, J. *J. Phys. Chem. Lett.* **2017**, *8*, 1402.
(45) Klotz, D. *Electrochem. Commun.* **2019**, *98*, 58.
(46) Ebadi, F.; Taghavinia, N.; Mohammadpour, R.; Hagfeldt, A.; Tress, W. *Nat. Commun.* **2019**, *10*, 1574.
(47) Chen, B.; Yang, M.; Zheng, X.; Wu, C.; Li, W.; Yan, Y.; Bisquert, J.; Garcia-Belmonte, G.; Zhu, K.; Priya, S. *J. Phys. Chem. Lett.* **2015**, *6*, 4693.
(48) Fecht, H. *Nature* **1992**, *356*, 133−135.
(49) Jiang, C.; Zheng, M.-J.; Morgan, D.; Szlufarska, I. *Phys. Rev. Lett.* **2013**, *111*, 155501.
(50) Rothmann, M. U.; Kim, J. S.; Borchert, J.; Lohmann, K. B.; O'Leary, C. M.; Sheader, A. A.; Clark, L.; Snaith, H. J.; Johnston, M. B.; Nellist, P. D.; Herz, L. M. *Science* **2020**, *370* (6516), 5940.
(51) Kim, M.; Ahn, N.; Cheng, D.; Xu, M.; Ham, S.; Pan, X.; Kim, S. J.; Luo, Y.; Fenning, D. P.; Tan, D. H. S.; Zhang, M.; Zhu, G.; Jeong, K.; Choi, M.; Meng, Y. S. Imaging real-time amorphization of hybrid perovskite solar cells under electrical biasing. UC San Diego, 2020. https://escholarship.org/uc/item/52x9k6tb (accessed Oct 23, 2020).

https://doi.org/10.1021/acsenergylett.1c01707
ACS Energy Lett. 2021, 6, 3530−3537